Soil Dynamics and Earthquake Engineering 119 (2019) 36–50

Contents lists available at ScienceDirect

Soil Dynamics and Earthquake Engineering

journal homepage: www.elsevier.com/locate/soildyn

MOCS-based optimum design of TMD and FTMD for tall buildings under near-field earthquakes including SSI effects

Sadegh Etedali[a,*], Morteza Akbari[b], Mohammad Seifi[b]

[a] Department of Civil Engineering, Birjand University of Technology, P.O. Box 97175-569, Birjand, Iran
[b] Independent researcher, Birjand, Iran

ARTICLE INFO

Keywords:
Tall buildings
Tuned mass damper
Friction tuned mass damper
Multi-objective cuckoo search
Soil-structure interaction
Energy

ABSTRACT

The use of TMDs is commonly discouraged for structures subjected to short-duration, pulse-like ground motions such as near-field earthquake excitations. Friction tuned mass damper (FTMD) is an innovative device compound of the traditional linear TMD with the idea of a friction damper which is still in the developmental stage for the seismic applications. The present paper investigates the performance of TMD and FTMD for seismic control of tall buildings under near-field earthquakes including soil-structure interaction (SSI) effects. A 40-story structure with a height-to-width ratio of four, a uniform mass distribution and a linear stiffness distribution in its height is considered in this study. Different conditions of the ground state are also considered for numerical studies. A design process based on a multi-objective cuckoo search (MOCS) algorithm is utilized for the optimum design of TMD and FTMD parameters. The simulation results indicate that ignoring the SSI effects may result in an inappropriate and unrealistic estimation of seismic responses and performance of TMD and FTMD in the high-rise structure. In terms of maximum displacement, acceleration, and drift of floors, it is found that the FTMD is capable of mitigating the structural responses better than the TMD. The efficiency of the FTMD is also compared with the TMD from the energy point of view for dissipation of the seismic input energy. The results show the superiority of the FTMD in the reduction of the maximum seismic input, kinetic and strain energies of the main structure, which confirm the capability of the FTMD being more than the TMD for mitigation of the seismic damages in the tall structure during near-field earthquakes. By increasing the soil softness, an increased trend is often achieved in the maximum seismic input and damage energies, thus ignoring the SSI effects may give an unrealistic result of the performance of TMD and FTMD in reducing the damage of seismic-excited tall buildings.

1. Introduction

TMD is one of the oldest passive control devices to enhance the safety of the tall structures and to improve the performance of the structures subjected to environmental dynamic loads. TMDs dissipate a portion of the seismic input energy and only a part of this energy is transferred to the main system. TMDs have been implemented in a number of high-rise buildings, towers, and bridges. Citigroup Center in New York City, Yokohama Landmark Tower in Yokohama, Burj Al Arab in Dubai, Trump World Tower in New York City, Taipei 101 in Taipei and The TV Tower in Berlin are some examples of the buildings equipped with TMD [1]. A TMD system consists of a mass, a spring, and a viscous damper. Optimal design of TMD parameters for a single degree of freedom (SDOF) system subjected to certain loads such as external harmonic force, harmonic base acceleration and etc. has been taken into account [2–7]. In these researches, it has been attempted to propose some formulations for optimum tuning of TMD for an SDOF system. However, these formulas are not advisable to use in the high-rise structures equipped with TMD because of the consideration of a single vibration mode in the optimum design process of TMD parameters. Moreover, they may not be suitable and applicable for seismic-excited structures. In addition, the only main purpose of the design of TMD is the reduction of the maximum displacement of the main system and the reduction of the maximum acceleration has not been considered in these methods. Hence, the evaluation of the performance of TMDs for mitigation of the seismic responses of the multi-story structures is still an important topic of research [8–12]. In recent years, some meta-heuristic based methods have been employed with the aim of overcoming the above-mentioned design problems. The superiority of meta-heuristic algorithms to the other methods in the literature has been reported [8–11,13,14]. The performance of TMDs in seismic-excited structures is often studied based on the rigid base assumption

* Corresponding author.
E-mail addresses: etedali@birjandut.ac.ir (S. Etedali), akbari69.project@gmail.com (M. Akbari), mohammad_seifi71@yahoo.com (M. Seifi).

https://doi.org/10.1016/j.soildyn.2018.12.027
Received 4 February 2018; Received in revised form 24 December 2018; Accepted 28 December 2018

without considering the SSI effects, whereas the SSI effects change the characteristics of the main structures such as natural frequencies, damping ratios, and shape modes [15]. Hence, some researchers attempt to study the SSI effects on the performance and time responses of the structures equipped with TMD. Jabari and Madabhushi [16] studied the soil-structure interaction effects on the structures retrofitted with TMDs. Farshidianfar and Soheili [13] employed an ant colony optimization algorithm for the optimum design of TMD in a 40-story structure subjected to earthquake excitations including SSI effects. Using the Lagrange method, Rahai et al. [17] proposed a mathematical model of a structure with TMD and SSI effects. In order to investigate the effects of TMDs on the responses of a multiple-story sway frame structure undergoing dynamic SSI, a series of geotechnical centrifuge tests were conducted [18]. Khatibinia et al. [14] utilized a multi-objective particle swarm optimization algorithm for optimal tuning of TMD parameters considering SSI effects. Employing two meta-heuristic algorithms, namely harmony search and bat algorithms, Bekdas and Nigdeli [19] proposed a meta-heuristic based optimization approach for the optimum design of TMDs considering SSI effects, too. The capability of TMD for energy dissipation is often related to the features of the input signal such as near/far fault, duration, and frequency content, whereas, for wind and other stationary loads, the effectiveness is well acknowledged and experienced [12]. TMDs may be effective against long-duration, narrow-band ground motions, whereas their use is commonly discouraged for short-duration, pulse-like ground motions such as near-field earthquake excitations [20–23]. A short-duration impulsive motion induces a high input energy at the beginning of the record [24]. Hence, there is little time to transfer energy from the primary structure into a TMD. On the other hand, they may result in large-amplitude, long-period pulses in the velocity and displacement time histories, which are especially a challenge for the safety of high-rise structures [23,25].

For a wide range of earthquakes with varying intensity and frequency content, the efficiency of passive TMDs can be improved using active and semi-active TMD devices [26–33], but the complexity and the high cost of the implementation of these devices for seismic-excited structures have led the researchers to enhance the performance of the existing passive TMD systems. A combined system of the traditional linear TMD with the idea of a friction damper, namely FTMD, is proposed to enhance the performance of the traditional TMDs. A portion of the energy is dissipated in the system through the mechanism of friction. Although many attempts have been made to investigate the design and application of the traditional linear TMDs, the study on the performance of the nonlinear FTMD for mitigation of the responses of the structures subjected to earthquake excitation is a topic that still inspires the efforts of researchers. Gewei and Basu [34] employed a statistical linearization method to analyze dynamic characteristics of a structure with FTMD system. Considering a five-story building under earthquake excitation, the efficiency of multiple friction tuned mass dampers is compared with a single FTMD in [35].

A performance decline of the traditional linear TMDs is detected in tall buildings subjected to near-field earthquakes. Hence, it is interesting to compare the performance of FTMD with that TMD for tall buildings during near-field earthquakes. The previous studies also indicate significant SSI effects on the seismic behavior of the structures. The SSI effects change the dynamic characteristics of the structures. While considering the rigid base assumption for the structures, these changes have been ignored in the design process of the FTMDs. On the other hand, the slip force of the FTMD as a passive device is a constant value. If the required slipping force is too high, FTMD will not slide and waste the energy for weak or moderate earthquakes. For a small slipping force, FTMD will not be able to adequately waste energy for strong earthquakes. As a result, the optimum tuning of the slip force of FTMD is a crucial and difficult issue in the design process. Moreover, the practical mass ratio, frequency ratio and damping ratio of FTMD are the other design parameters of the FTMD. Meta-heuristic algorithms are able to solve optimization problems without the need for a continuous and differentiable function. Furthermore, they are able to handle complex optimization problems and take into account the nonlinearities of the problems. Passive friction devices may reduce the displacement of floors at the cost of an increase in the acceleration of floors. A meta-heuristic multi-objective optimization algorithm can be used to create an optimal balance between the reductions of two important structural responses. To the best knowledge of the authors, there is no study on multi-objective optimization of the FTMD parameters for tall buildings under near-field earthquakes including SSI effects. The present study proposes a design process based on a MOCS algorithm for the optimum design of FTMD parameters in seismic-excited structures including SSI effects. A 40-story structure in three cases of the uncontrolled structure, the structure equipped with TMD, and the structure equipped with FTMD is adopted for numerical studies. The governing differential equations of motion of the structures equipped with FTMD including SSI effects are formulated for time history analyses subjected to earthquake excitations. In addition to the fixed base case, three types of soils including soft, medium, and dense are considered for investigation the SSI effects on the seismic performance of TMD and FTMD. A MOCS algorithm is utilized as a powerful tool for optimum tuning of the TMD and FTMD parameters. In the end, the performances of TMD and FTMD are compared with the structure subjected to four well-known earthquake excitations. Furthermore, the effectiveness of FTMD is compared with TMD from the energy point of view.

The rest of the paper is organized as follows. A mathematical model of a tall structure equipped with an FTMD including SSI effects is developed in Section 2. Section 3 gives a brief overview of the MOCS algorithm. The optimum designs of the TMD and FTMD parameters for a 40-story building subjected to earthquake excitations are carried out in Section 4. The simulation results are given in Section 5. The concluding remarks are summarized in Section 6.

2. The governing equation of motion for the structure equipped with FTMD including SSI effects

An N story equipped with an FTMD, situated on the top floor, including SSI effects, can be simulated as a shear building model. In this case, N–degree of freedom can be assigned to the main structure (See Fig. 1). The FTMD parameters including mass, viscous damping and stiffness are represented by M_{FTMD}, $C_{FTMD,}$ and K_{FTMD}, respectively. By attaching an FTMD to the main structure, only the degree-of-freedom of the main structure is added by one. On the other hand, two degree-of-freedoms are also added to the structural model for displacement and rotation of the foundation when SSI effects are considered. Hence, an $N+3$ degree-of-freedom system, shown in Fig. 1, can be described as the structural model equipped with FTMD considering SSI effects.

Using the Lagrangian method, the equations of motion of the N-story structure including SSI effects, equipped with an FTMD located on the roof of the building, can be outlined as follows [35,36]:

$$[m]\{\ddot{x}(t)\} + [c]\{\dot{x}(t)\} + [k]\{x(t)\} = -[m^*]\{1\}\ddot{u}_g + \{b\}F_s(t) \quad (1)$$

where $[m]$, $[c]$, and $[k]$ represent the mass, damping and stiffness matrices of the structure, respectively. The vectors $\{\ddot{x}(t)\}$, $\{\dot{x}(t)\}$, $\{x(t)\}$ are the acceleration, velocity, and displacement vectors of the system, in the order mentioned. Also, $[m^*]$ represents the matrix of acceleration mass for earthquake and $\ddot{u}_g$ shows the ground acceleration. Moreover, $\{1\}$ and $\{b\}$ are the location vectors for the seismic excitation and friction force of the FTMD. In addition, $F_s(t)$ denotes the friction force generated by the FTMD. Using the Lagrange's equation, the mass matrix is obtained by the following form:

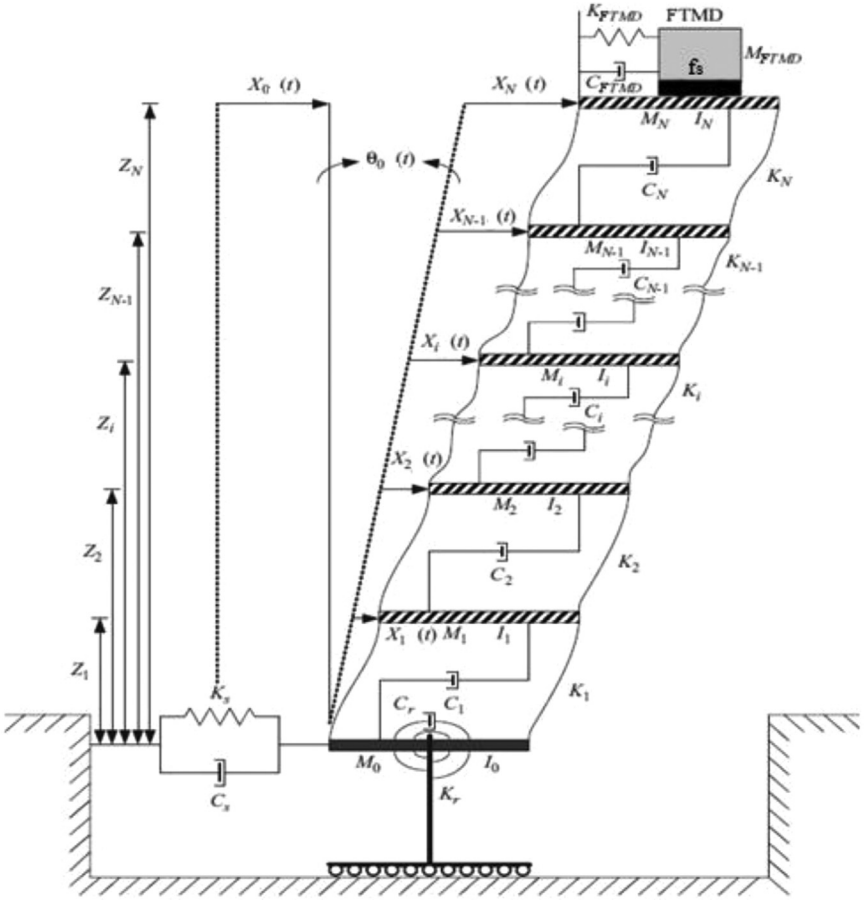

Fig. 1. A mathematical model of an *N*-story structure equipped with an FTMD including SSI effects.

Table 1
Structural parameters of the 40-story building [23].

No. of stories	40
Story height	4 m
Story mass (M_i, i = 1,...,40)	9.8×10^5 kg
Story mass moment of inertia (I_i,i = 1,...,40)	1.31×10^8 kg m^2
Story stiffness ($K_1 < K_i < K_{40}$)	$K_1 = 2.13 \times 10^9$ N/m, $K_{40} = 9.98 \times 10^8$ N/m
Foundation mass (M_0)	1.96×10^6 kg
Foundation mass moment of inertia (I_0)	1.96×10^8 kg m^2

$$[m] = \begin{bmatrix} [M]_{N\times N} & \{0\}_{N\times 1} & \{M\}_{N\times 1} & \{MZ\}_{N\times 1} \\ & M_{FTMD} & M_{FTMD} & M_{FTMD}Z_N \\ & & M_0 + \Sigma_{j=1}^{N}(M_j) + M_{FTMD} & \Sigma_{j=1}^{N}(M_jZ_j) + M_{FTMD}Z_N \\ Sym. & & & I_0 + \Sigma_{j=1}^{N}\left(I_j + M_jZ_j^2\right) \\ & & & + M_{FTMD}Z_N^2 \end{bmatrix} \quad (2)$$

in which

$$[M]_{N\times N} = \begin{bmatrix} M_1 & 0 & 0 & 0 & 0 \\ & M_2 & 0 & 0 & 0 \\ & & \ddots & \{0\} & \{0\} \\ & & & M_{N-1} & 0 \\ Sym. & & & & M_N \end{bmatrix} \{M\}_{N\times 1} = \begin{Bmatrix} M_1 \\ M_2 \\ \vdots \\ M_{N-1} \\ M_N \end{Bmatrix} \{MZ\}_{N\times 1} = \begin{Bmatrix} M_1Z_1 \\ M_2Z_2 \\ \vdots \\ M_{N-1}Z_{N-1} \\ M_NZ_N \end{Bmatrix} \quad (3)$$

where M_j, I_j and Z_j (j = 1, ...,N) refer to the mass, mass moment of inertia, and the elevation of the j-th floor. Also, M_0 and I_0 denote the mass and mass moment of inertia of the foundation. Moreover, the damping and stiffness matrices can be given by:

$$[c] = \begin{bmatrix} [C]_{N\times N} & \begin{Bmatrix} 0_{(N-1)\times 1} \\ -C_{FTMD} \end{Bmatrix} & \{0\}_{N\times 1} & \{0\}_{N\times 1} \\ & C_{FTMD} & 0 & 0 \\ & & C_s & 0 \\ Sym. & & & C_r \end{bmatrix} \quad (4)$$

Table 2
Parameters of the soils and foundation [23].

Soil type	Poisson's ratio, (ν_s)	Soil density, ρ_s (kg/m^3)	Shear-wave velocity, V_S (m/s)	Shear modulus, G_s (N/m^2)	Swaying damping, C_s ($N.s/m$)	Rocking damping, C_r ($N.s.m$)	Swaying stiffness, K_s (N/m)	Rocking stiffness, K_r ($N.m$)
Soft	0.49	1800	100	1.80×10^7	2.19×10^8	2.26×10^{10}	1.91×10^9	7.53×10^{11}
Medium	0.48	1900	300	1.71×10^8	6.90×10^8	7.02×10^{10}	1.80×10^{10}	7.02×10^{12}
Dense	0.33	2400	500	6.00×10^8	1.32×10^9	1.15×10^{11}	5.75×10^{10}	1.91×10^{13}

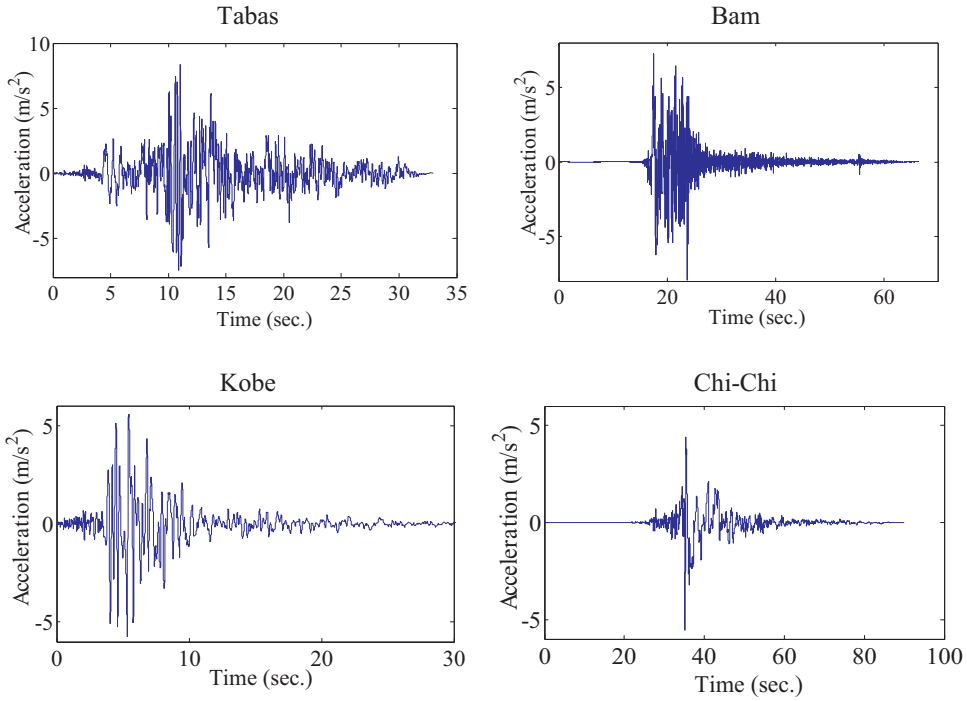

Fig. 2. Time histories of the acceleration of Tabas, Bam, Kobe, and Chi -Chi earthquakes.

$$[k] = \begin{bmatrix} [K]_{N\times N} & \begin{Bmatrix} 0_{(N-1)\times 1} \\ -K_{FTMD} \end{Bmatrix} & \{0\}_{N\times 1} & \{0\}_{N\times 1} \\ & K_{FTMD} & 0 & 0 \\ & & K_s & 0 \\ Sym. & & & K_r \end{bmatrix} \tag{5}$$

where

$$[C]_{N\times N} = \begin{bmatrix} C_1 + C_2 & -C_2 & 0 & 0 & 0 \\ & C_2 + C_3 & \ddots & \vdots & 0 \\ & & \ddots & -C_{N-1} & \vdots \\ & & & C_{N-1} + C_N & -C_N \\ Sym. & & & & C_N + C_{FTMD} \end{bmatrix} \tag{6}$$

$$[K]_{N\times N} = \begin{bmatrix} K_1 + K_2 & -K_2 & 0 & 0 & 0 \\ & K_2 + K_3 & \ddots & \vdots & 0 \\ & & \ddots & -K_{N-1} & \vdots \\ & & & K_{N-1} + K_N & -K_N \\ Sym. & & & & K_N + K_{FTMD} \end{bmatrix} \tag{7}$$

in which, the swaying damping and rocking damping of the foundation are denoted by C_s and C_r. Similarly, K_r and K_s represent the rocking and swaying stiffness of the foundation. Also, K_j and C_j ($j = 1, ...,N$) are the stiffness and damping of the j-th floor. The acceleration mass matrix, [m*], can be obtained as follows:

$$[m^*] = \begin{bmatrix} [M]_{N\times N} & \{0\}_{N\times 1} & \{0\}_{N\times 1} & \{0\}_{N\times 1} \\ & M_{FTMD} & 0 & 0 \\ & & M_0 + \Sigma_{j=1}^{N}(M_j) + M_{FTMD} & 0 \\ Sym. & & & \Sigma_{j=1}^{N}(M_j Z_j) + M_{FTMD} Z_N \end{bmatrix} \tag{8}$$

In addition, the displacement vector $\{x(t)\}$ includes the relative displacement of floors, $x_j(t)$, ($j = 1, ...,N$), the foundation displacement, $x_0(t)$, and the foundation rotation, $\theta_0(t)$, as well as the FTMD displacement, $x_{FTMD}(t)$, as follows:

$$\{x(t)\} = \begin{Bmatrix} x_1(t) \\ x_2(t) \\ \vdots \\ x_N(t) \\ x_{FTMD}(t) \\ x_0(t) \\ \theta_0(t) \end{Bmatrix} \tag{9}$$

Also, the location vector of the friction force of the FTMD can be given by:

$$\{b\} = \begin{Bmatrix} 0 \\ 0 \\ \vdots \\ 1 \\ -1 \\ 0 \\ 0 \end{Bmatrix} \tag{10}$$

The friction force of the FTMD, F_s, is given by the following equation

$$\mathrm{F_s} = \mathrm{f_s sgn}(\dot{\mathrm{X}}_{\mathrm{FTMD}} - \dot{\mathrm{X}}_{\mathrm{N}}) \tag{11}$$

where $\dot{X}_{FTMD}$ refers to the velocity of the FTMD and $\dot{X}_N$ represents the velocity of the top floor. The limited frictional force or slip force, $\mathrm{f_s}$, can be stated in a normalized form by a coefficient of friction:

$$\mathrm{R_f} = \frac{f_s}{M_{FTMD}.\, g} \tag{12}$$

where $\mathrm{M_{FTMD}}$, g, and R_f represent the mass of FTMD, gravitational acceleration, and the coefficient of friction, respectively.

Additionally, the damper force can be also given by the following equation [35]:

$$F_s = \mathrm{f_s} Z \tag{13}$$

where $\mathrm{f_s}$ denotes the limiting friction force or slip force of the damper and Z is the non-dimensional hysteretic component, which satisfies the following first-order non-linear differential equation.

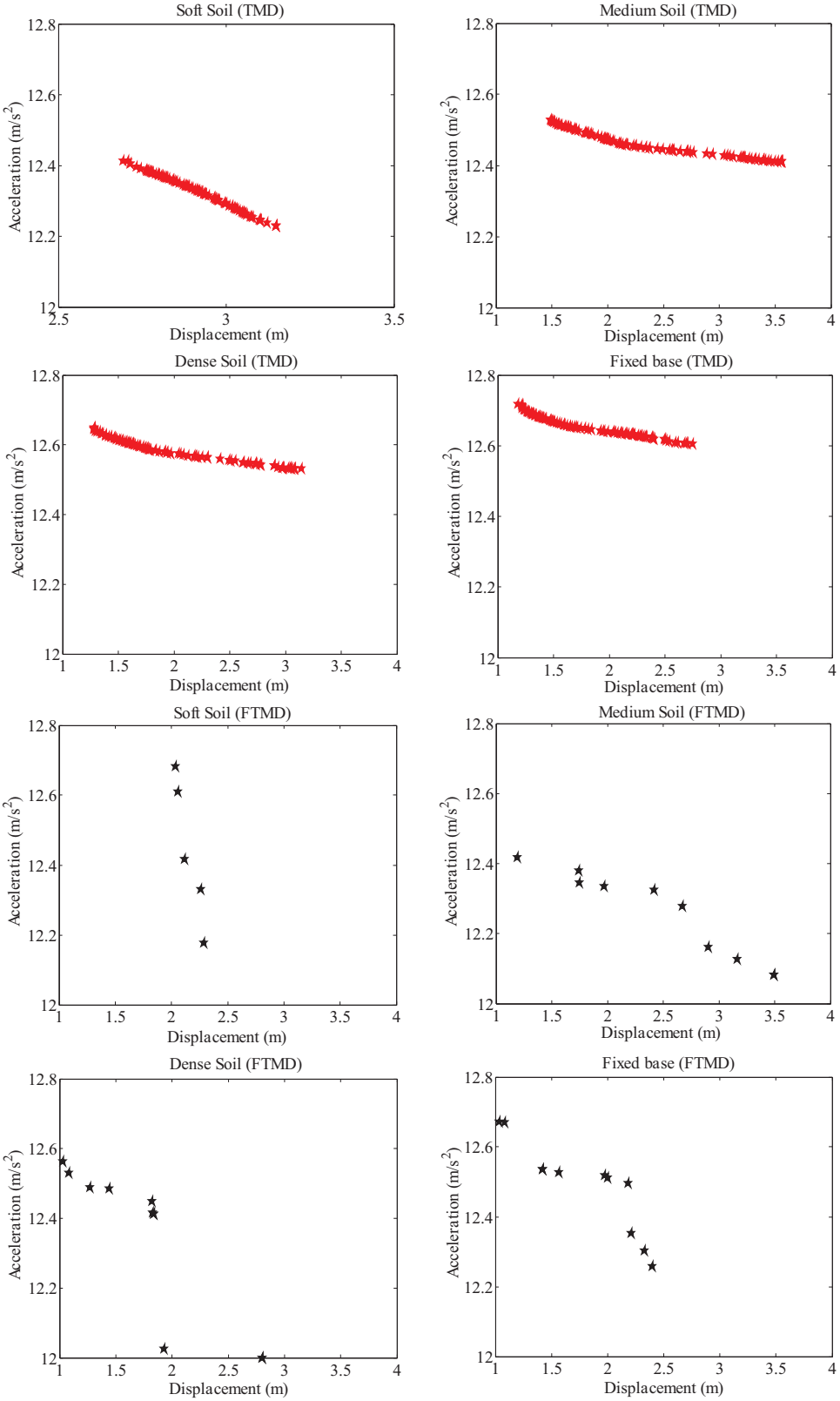

Fig. 3. The Pareto-optimal front diagrams for optimum tuning of TMD and FTMD parameters of the building subjected to Tabas earthquake.

$$q\frac{dz}{dt} = A(\dot{X}_{FTMD} - \dot{X}_N) - \beta|\dot{X}_{FTMD} - \dot{X}_N|Z|Z|^{n-1} - \tau(\dot{X}_{FTMD} - \dot{X}_N)|Z|^n \quad (14)$$

where q is the yield displacement of the frictional force loop, and A, β, τ, and n are non-dimensional parameters of the hysteretic loop, which control the shape of the loop. The values of the parameters are considered in such a way that it provides typical Coulomb-friction damping. [37].

By elimination of the term $\{b\}F_s(t)$ from Eq. (1), one can extract the governing equation of motion for the structure equipped with TMD

Table 3
Optimum parameters of TMD and FTMD.

Earthquakes	Soil type	TMD		FTMD		
		C_{TMD} $(MN.\ s/m)$	K_{TMD} (MN/m)	C_{FTMD} $(MN.\ s/m)$	K_{FTMD} (MN/m)	f_s (MN)
Tabas	Soft	1.0336	3.4069	0.8739	2.7705	2.5015
	Medium	0.0462	2.7271	0.7712	2.6811	3.5167
	Dense	0.0455	2.6379	0.9227	2.7952	3.0995
	Fixed base	0.0453	2.6194	0.6800	2.6741	2.0804
Bam	Soft	1.1216	4.2943	0.8045	2.7908	1.3228
	Medium	1.6578	9.0883	0.3868	3.4750	0.8133
	Dense	0.0674	5.7996	0.9416	3.2864	0.8037
	Fixed base	0.0486	10.3360	0.0653	5.4533	0.4807
Kobe	Soft	0.1563	3.3290	1.1415	4.1553	0.7768
	Medium	0.0638	5.1884	0.8019	4.9671	0.9402
	Dense	0.0622	4.9324	1.2338	4.8541	1.6439
	Fixed base	0.0601	4.6043	1.1205	4.4694	1.0940
Chi-Chi	Soft	0.0508	3.2914	0.4948	1.6832	1.6709
	Medium	0.0507	3.2850	0.6601	3.5566	1.0056
	Dense	0.0499	3.1824	1.0451	1.0435	2.9034
	Fixed base	0.0492	3.0878	0.8686	4.9455	3.0668

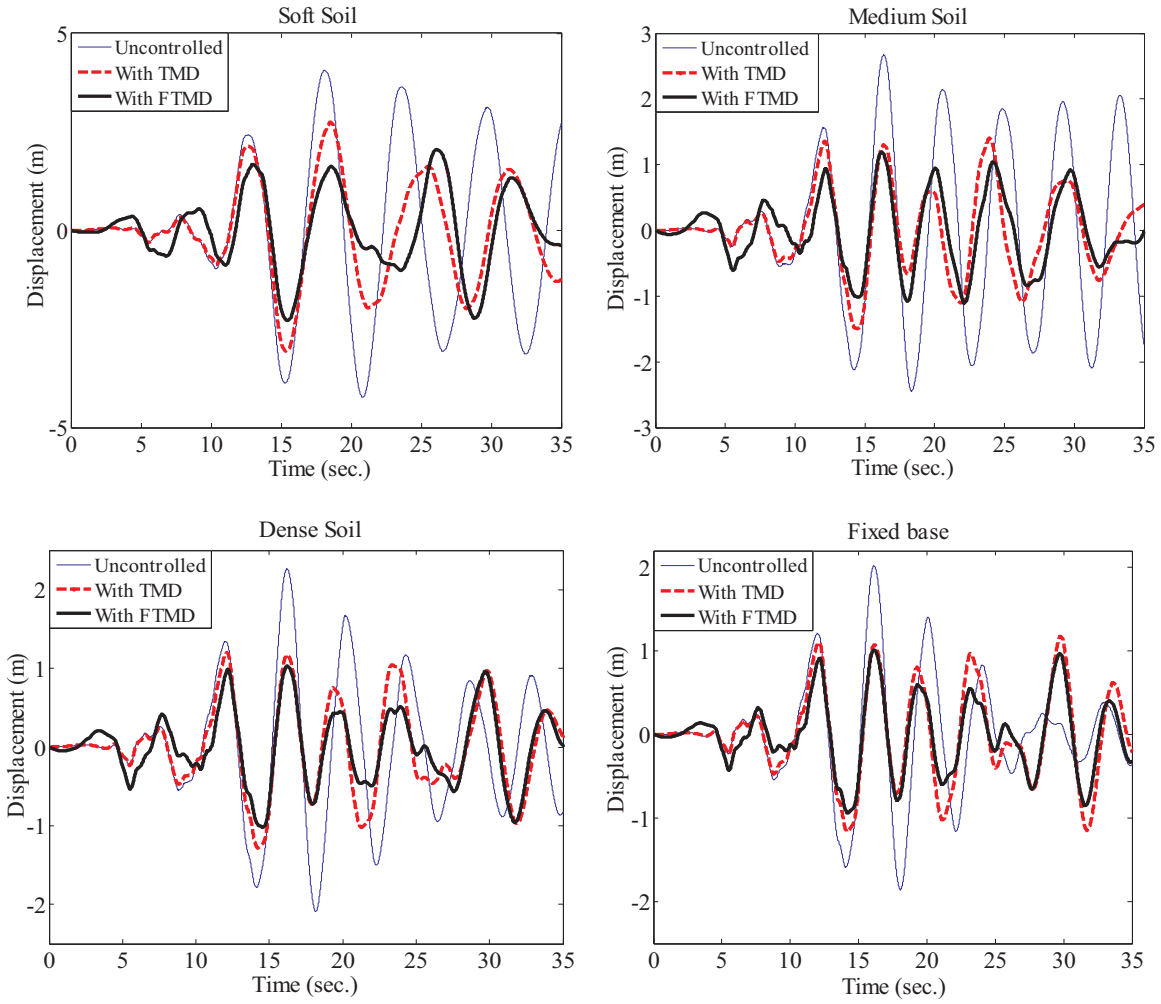

Fig. 4. Time histories of the top floor displacement during Tabas earthquake.

including SSI effects.

3. A Multi-objective cuckoo search algorithm

CS algorithm was firstly introduced by Yang and Deb [38] to solve optimization problems. Two important features in CS algorithm make it superior to many other meta-heuristic algorithms. First, the CS algorithm applies Lévy flights, which are far more efficient than the simple random walks. The Lévy flight has an infinite mean and variance. Therefore, it can explore the search space better than a standard Gaussian process [39–41]. The CS also provides larger moves for a global search; therefore, new moves can cover more extensive regions

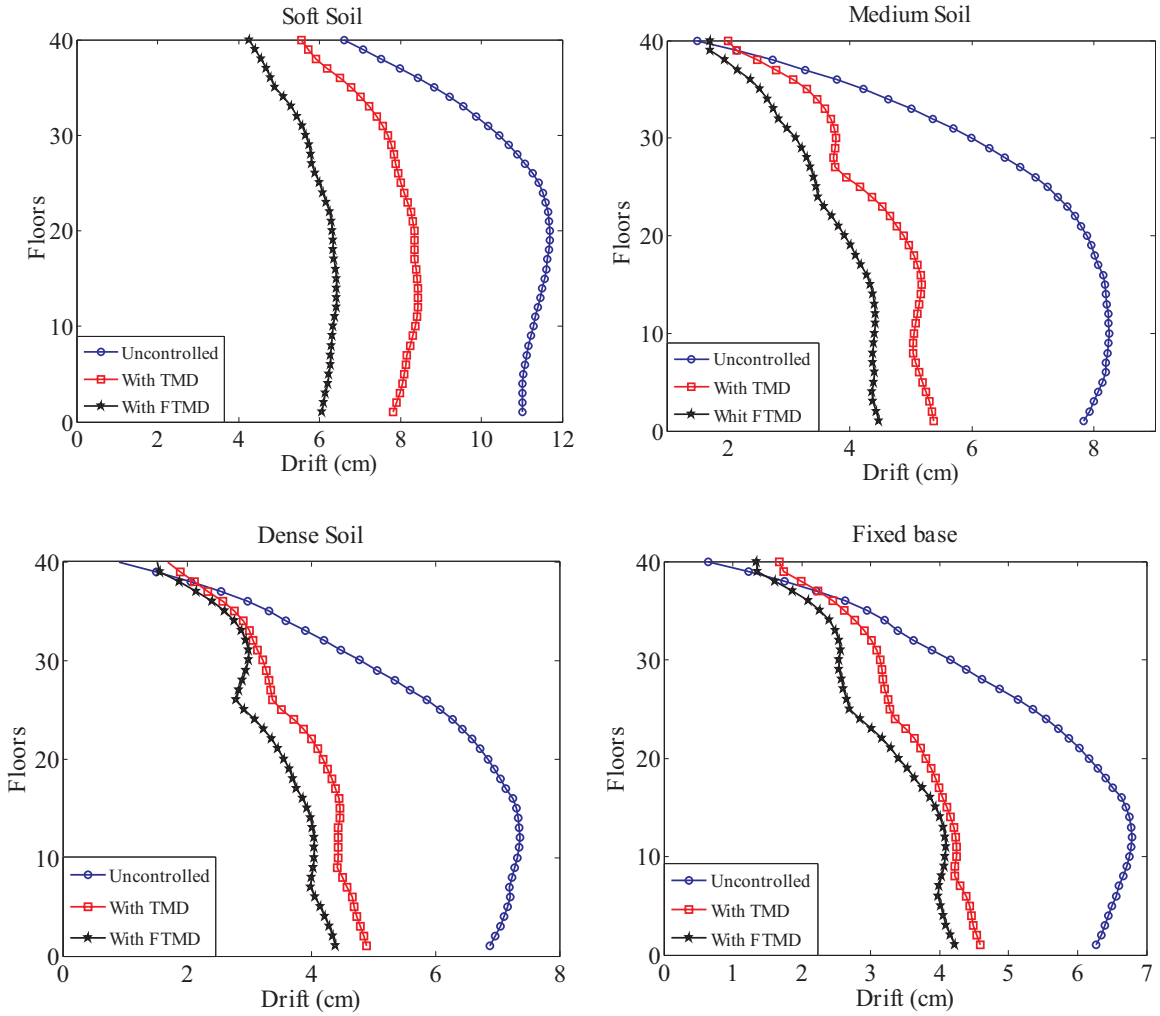

Fig. 5. The maximum drift of floors during Tabas earthquake.

[41].

Some configurable parameters of the CS include population size n, switching probability p_a, step-size α, and Lévy flights exponent β. The Lévy flights exponent and step-size can be set as constants without affecting much the performance of the algorithm, whereas the population size and switching probability are the main parameters of the CS. Therefore, the CS has fewer algorithm-dependent parameters in comparison with other algorithms. For most problems, α and β are considered as constant values 0.1 and 1.5, whereas p_a and n are variable and have great effects on the performance of the algorithm. Switching probability provides balance between local and global optimization. By increasing p_a, the probability of global optimization is reduced and vice versa [38,39]. Considering the advantages of the CS in terms of ease of implementation, few parameters to tune, and fast convergence rate, it provides a better performance in comparison with a number of existing algorithms such as PSO and GA [39]. Civicioglu and Besdok [42] reported that a higher degree of robustness is provided by the CS in comparison with PSO and ABC algorithms. According to the principles based on the single objective CS, Yang and Deb [41] developed a MOCS for optimization problems with conflicting objectives. The performance of the MOCS algorithm was compared with several well-known multi-objective optimization algorithms such as NSGA-2. It was shown that the convergence of MOCS was the highest and it led to better solutions in a more efficient way [41]. Recently, MOCS has successfully been used in the area of structural and earthquake engineering applications [43–51].

In the MOCS, the following rules are used for a problem with K objectives [41]:

- Each cuckoo lays K eggs at a time and dumps them in a randomly chosen nest. This rule simulates a randomization process so that a new solution can be randomly generated either by a random walk or by a Lévy flight. It also performs a localized random permutation and can be considered as a form of crossover. For each nest, there can be K solutions, which are generated according to Eq. (15).
- The best nests with a high quality of eggs (solutions) will carry over to the next generations. The second rule corresponds with elitism.
- Each nest will be abandoned with a probability $p_a \in [0,1]$ and a new nest with K eggs will be built according to the similarities/differences of the eggs. In order to generate diversity, some random mixing can be used. Hence, it can play the role of mutation.

Based on these three rules, the basic steps of the MOCS can be summarized as follows.

$$x_i^{t+1} = x_i^t + \alpha \quad \oplus \text{Lévy}(\beta) \tag{15}$$

The product ⊕ is entry-wise multiplications and β refers to the Lévy flights exponent. Also, α is the step size and can be given by:

$$\alpha = \alpha_0 \oplus (x_j^t - x_i^t) \tag{16}$$

in which x_j^t and x_i^t are two different randomly selected solutions. The generation of step size is performed using Lévy flights. A simple scheme

Table 4
Maximum structural responses for different conditions of the ground.

Earthquake	Soil type	Unctrl.	TMD	FTMD	TMD	FTMD
Tabas		Maximum floor Displacement (m)			Reduction (%)	
	Soft	4.23	3.06	2.29	27.66	45.86
	Medium	2.67	1.50	1.19	43.82	55.43
	Dense	2.26	1.28	1.03	43.36	54.42
	Fixed base	2.02	1.18	1.01	41.58	50.00
		Maximum floor Acceleration (m/s^2)			Reduction (%)	
	Soft	12.29	12.26	12.18	0.24	0.90
	Medium	12.54	12.53	12.42	0.08	0.96
	Dense	12.68	12.65	12.56	0.24	0.95
	Fixed base	12.76	12.72	12.67	0.31	0.71
		Maximum drift of floors (cm)			Reduction (%)	
	Soft	11.69	8.44	6.43	27.80	45.00
	Medium	8.25	5.38	4.47	34.79	45.82
	Dense	7.36	4.89	4.39	33.56	40.35
	Fixed base	6.79	4.59	4.21	32.40	38.00
Bam		Maximum floor Displacement (m)			Reduction (%)	
	Soft	0.85	0.80	0.68	5.88	20.00
	Medium	0.89	0.83	0.62	6.74	30.34
	Dense	0.88	0.84	0.69	4.55	21.60
	Fixed base	0.88	0.83	0.70	5.68	20.45
		Maximum floor Acceleration (m/s^2)			Reduction (%)	
	Soft	9.37	9.18	9.13	2.03	2.56
	Medium	9.64	9.59	9.42	0.52	2.28
	Dense	10.17	10.19	10.08	-0.20	0.88
	Fixed base	10.36	10.32	10.13	0.39	2.22
		Maximum drift of floors (cm)			Reduction (%)	
	Soft	4.76	4.52	4.11	5.04	13.66
	Medium	4.49	4.23	3.76	5.79	16.26
	Dense	4.40	4.22	3.86	4.09	12.27
	Fixed base	4.34	4.11	3.94	5.30	9.22
Kobe		Maximum floor Displacement (m)			Reduction (%)	
	Soft	0.55	0.50	0.40	9.09	27.27
	Medium	0.71	0.58	0.37	18.31	47.89
	Dense	0.70	0.58	0.41	17.14	41.43
	Fixed base	0.69	0.58	0.39	15.94	43.48
		Maximum floor Acceleration (m/s^2)			Reduction (%)	
	Soft	8.43	8.43	8.29	0.00	1.66
	Medium	8.97	8.96	8.88	0.11	1.00
	Dense	9.19	9.17	9.00	0.22	2.07
	Fixed base	9.21	9.20	8.98	0.11	2.50
		Maximum drift of floors (cm)			Reduction (%)	
	Soft	2.92	2.81	2.53	3.77	13.36
	Medium	3.22	2.83	2.46	12.11	23.60
	Dense	3.17	2.82	2.37	11.04	25.24
	Fixed base	3.12	2.80	2.30	10.26	26.28
Chi-Chi		Maximum floor Displacement (m)			Reduction (%)	
	Soft	3.80	3.38	2.58	11.05	32.11
	Medium	2.62	2.36	2.04	9.92	22.14
	Dense	2.42	2.19	1.77	9.50	26.86
	Fixed base	2.29	2.09	1.17	8.73	48.91
		Maximum floor Acceleration (m/s^2)			Reduction (%)	
	Soft	6.09	6.07	6.07	0.33	0.33
	Medium	8.38	7.62	7.11	9.07	15.16
	Dense	9.76	8.74	7.97	10.45	18.34
	Fixed base	10.55	9.44	9.22	10.52	12.61
		Maximum drift of floors (cm)			Reduction (%)	
	Soft	10.60	9.62	7.60	9.25	28.30
	Medium	8.44	7.67	6.84	9.12	18.96
	Dense	7.83	7.19	5.47	8.17	30.14
	Fixed base	7.41	6.87	4.28	7.29	42.24

Table 5
The average reduction values of maximum structural responses for all studied earthquakes with respect to the corresponding uncontrolled cases.

Soil type	The average reduction values in the term of the maximum floor displacement		maximum floor acceleration		maximum drift of floor	
	TMD	FTMD	TMD	FTMD	TMD	FTMD
Soft	13.42%	31.31%	0.65%	1.36%	11.47%	25.08%
Medium	19.70%	38.95%	2.45%	4.85%	15.45%	26.16%
Dense	18.64%	36.08%	2.68%	5.56%	14.22%	27.00%
Fixed base	17.89%	40.71%	2.84%	4.51%	13.81%	28.94%

is summarized in Eq. (17):

$$s = \alpha_0 \oplus (x_j^t - x_i^t) \oplus \text{Lévy}(\beta) = 0.01 \ (x_j^t - x_i^t) \frac{u}{|v|^{\frac{1}{\beta}}} \tag{17}$$

Furthermore, u and v are given by the normal distributions as follows:

$$u \sim N(0,\sigma_u^2), v \sim N(0,\sigma_v^2) \tag{18}$$

where σ_u and σ_v are as shown in the following equation:

$$\sigma_u = \left\{ \frac{G(1+\beta)\sin(\pi\beta/2)}{G[(1+\beta)/2]\beta 2^{(\beta-1)/2}} \right\}^{1/\beta}, \quad \sigma_v = 1 \tag{19}$$

where G is the standard Gamma function. In essence, the second rule is an elitism strategy and passes the best solutions onto the next generation. This strategy helps the algorithm to accelerate its converge speed. Finally, the third rule is a mutation operator and discards the worst solutions with a probability. Eq. (20) indicates how a new solution x_i^{t+1} is generated using a simple random walk.

$$x_i^{t+1} = x_i^t + \alpha_0 \oplus H(p_a - \epsilon) \oplus (x_j^t - x_k^t) \tag{20}$$

in which H is the Heaviside function; α_0 represents the step size scaling factor, and ϵ is a random number with uniform distribution [41].

4. Numerical studies

A 40-story structure, introduced in [13,14,19,52], is considered to investigate the seismic behavior of tall buildings equipped with FTMD including SSI effects. Breadth, depth, and height of the structure are 40, 40, and 160 m, respectively. Furthermore, it is assumed that the foundation of the structures is located on three types of ground states: soft, medium and dense. The case of the structure with a fixed-base is also considered in the numerical studies. Each story is assumed to have the same mass, height, and moment of inertia. The stiffness of the structure linearly decreases when Z_j distances increase (See Fig. 1). Table 1 indicates the properties of the structures. The fundamental frequency of the fixed-base building is calculated as 1.64 rad/s. The fundamental frequencies of the structure for dense, medium, and soft soil cases are 1.61 rad/s, 1.54 rad/s and 1.09 rad/s, respectively.

Classical Rayleigh damping is adapted to form the damping matrix of the main structure. Based on Rayleigh damping, the damping matrix of the main structure, $[C]_{N\times N}$, can be expressed as a linear combination of the mass and stiffness matrices of the main structure as follows:

$$[C]_{N\times N} = \alpha[M]_{N\times N} + \beta[K]_{N\times N} \tag{21}$$

in which α and β are the coefficients of the Rayleigh damping matrix which are 0 and 0.02, respectively [13,14,52]. Table 2 shows the parameters of the soil and foundation for the three types of soils.

In order to mitigate the structural damages of a high-rise structure, the reduction of the large displacements of the floors is always at the center of attention of the designers. On the other hand, to enhance the comfort/serviceability and to mitigate the non-structural damages, the

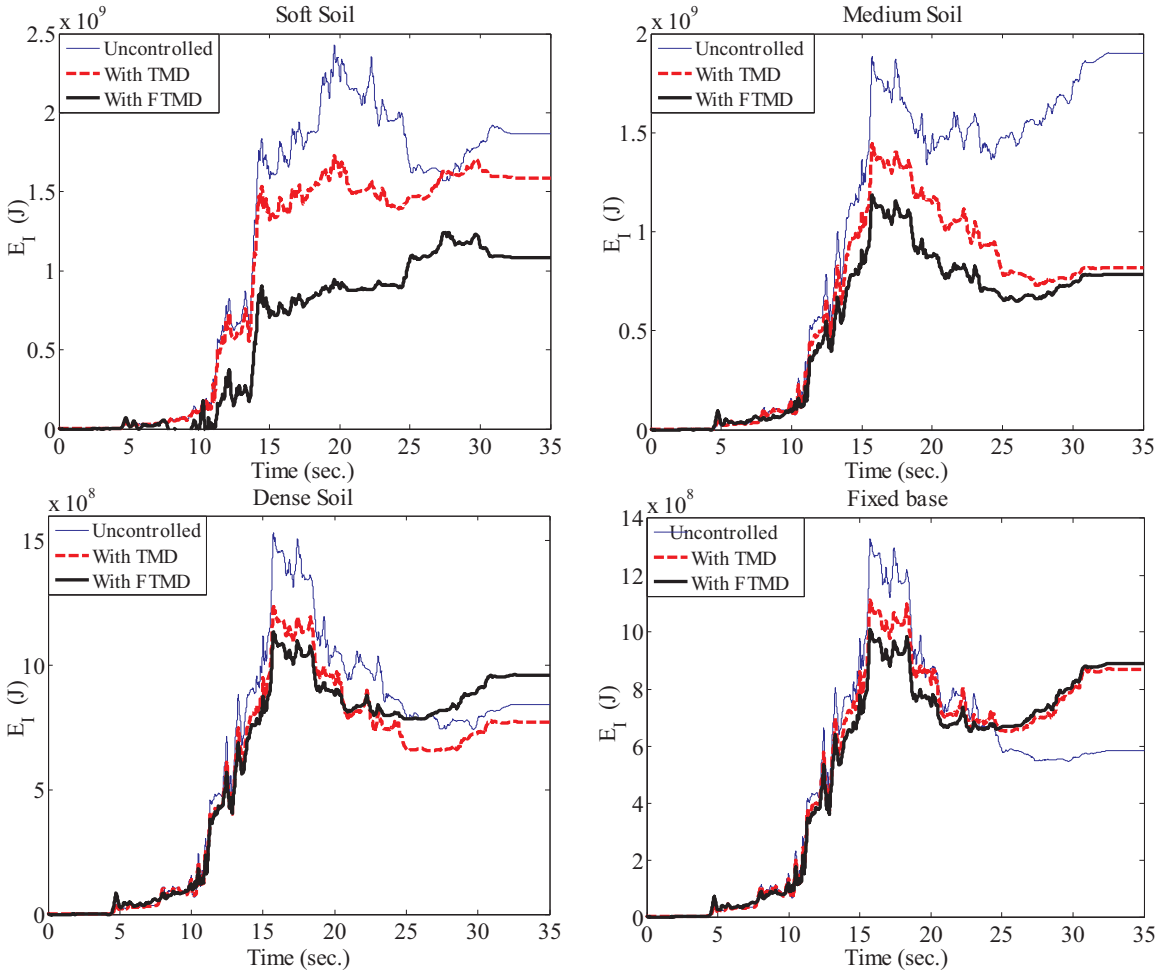

Fig. 6. Time histories of the seismic input energy during Tabas earthquake for different conditions of the ground.

reduction of maximum acceleration of stories, especially for tall buildings, is an important issue for designers. Passive friction devices may reduce the displacement of floors at the cost of an increase in the acceleration of floors. An optimum design of TMD and FTMD systems for the seismic control of the high-rise structures should be considered as a multi-objective optimization problem. Optimization problems with many local optimums (multi-modal problems) require heavier search, and hence, more time may be required. To cope with such problems, an efficient tool is a meta-heuristic algorithm with enough diversity of solutions. On the other hand, multi-objective optimization algorithms are able to create a suitable trade-off between the conflicting objectives and generate a set of possible solutions for designers, which form the so-called Pareto front. This advantage provides the possibility to choose the best solution from among the presented ones. In other words, the designer can select a possible solution that better agrees with the designer's own decisions. In this paper, a MOCS algorithm is employed for optimal tuning of TMD and FTMD parameters. Hence, two multi-objective optimization problems are defined for this purpose.

The first optimization problem is defined for optimum design of TMD parameter, including optimum frequency ratio, f_{TMD}^{opt}, and optimum damping ratio, ξ_{TMD}^{opt}, as follows:

$$\begin{aligned} &\{\textit{Find}:\ f_{TMD}^{opt} \text{ and } \xi_{TMD}^{opt}\\ &\text{minimize:}\ \max(\ max x_i(t)\ ) \text{and } \max(\ max\|\ddot{x}_i(t)\|\ )\ i = 1, \ldots, N\\ &\textit{Subjected to}:\ 0.6 \ll f_{TMD} \ll 1.4 \text{ and } 0.01 \ll \xi_{TMD} \ll 0.2 \end{aligned} \tag{22}$$

where $max\|x_i(t)\|$ and $max\,\|\ddot{x}_i(t)\|$represent the maximum displacement and acceleration of the i-th floor, respectively. For a preselected mass ratio of TMD, γ, the TMD mass, optimum damping, and stiffness are calculated as:

$$\begin{cases} M_{TMD} = \gamma M_s\\ C_{TMD} = 2M_{TMD}\xi_{TMD}^{opt} f_{TMD}^{opt}\omega_s\\ K_{TMD} = M_{TMD}(f_{TMD}^{opt}\omega_s)^2 \end{cases} \tag{23}$$

in which $M_s = \sum_{i=1}^{N} M_i$ is the total mass of the structure and ω_s is the fundamental frequency of the structure.

For optimum design of FTMD parameters, the second optimization problem is defined as the following equation:

$$\begin{aligned} &\{\textit{Find}:\ f_{FTMD}^{opt},\ \xi_{FTMD}^{opt} \text{ and } R_f^{opt}\\ &\text{minimize:}\ \max(\ max x_i(t)\ ) \text{and } \max(\ max\|\ddot{x}_i(t)\|\ )\ i = 1, \ldots, N\\ &\textit{Subjected to}:\ 0.6 \ll f_{FTMD} \ll 1.4,\ 0.01 \ll \xi_{FTMD} \ll 0.2 \text{ and } 0.01 \ll R_f \ll 0.5 \end{aligned} \tag{24}$$

The optimum damping, stiffness, and slip force of the FTMD for a preselected mass ratio of FTMD, γ, can be given by:

$$\begin{cases} M_{FTMD} = \gamma M_s\\ C_{FTMD} = 2M_{FTMD}\xi_{FTMD}^{opt} f_{FTMD}^{opt}\omega_s\\ K_{FTMD} = M_{FTMD}\,(f_{FTMD}^{opt}\omega_s)^2\\ f_s = R_f^{opt} M_{FTMD} g \end{cases} \tag{25}$$

in which g is the gravitational acceleration. From a practical standpoint and carrying out a fair comparison of the seismic performance of TMD

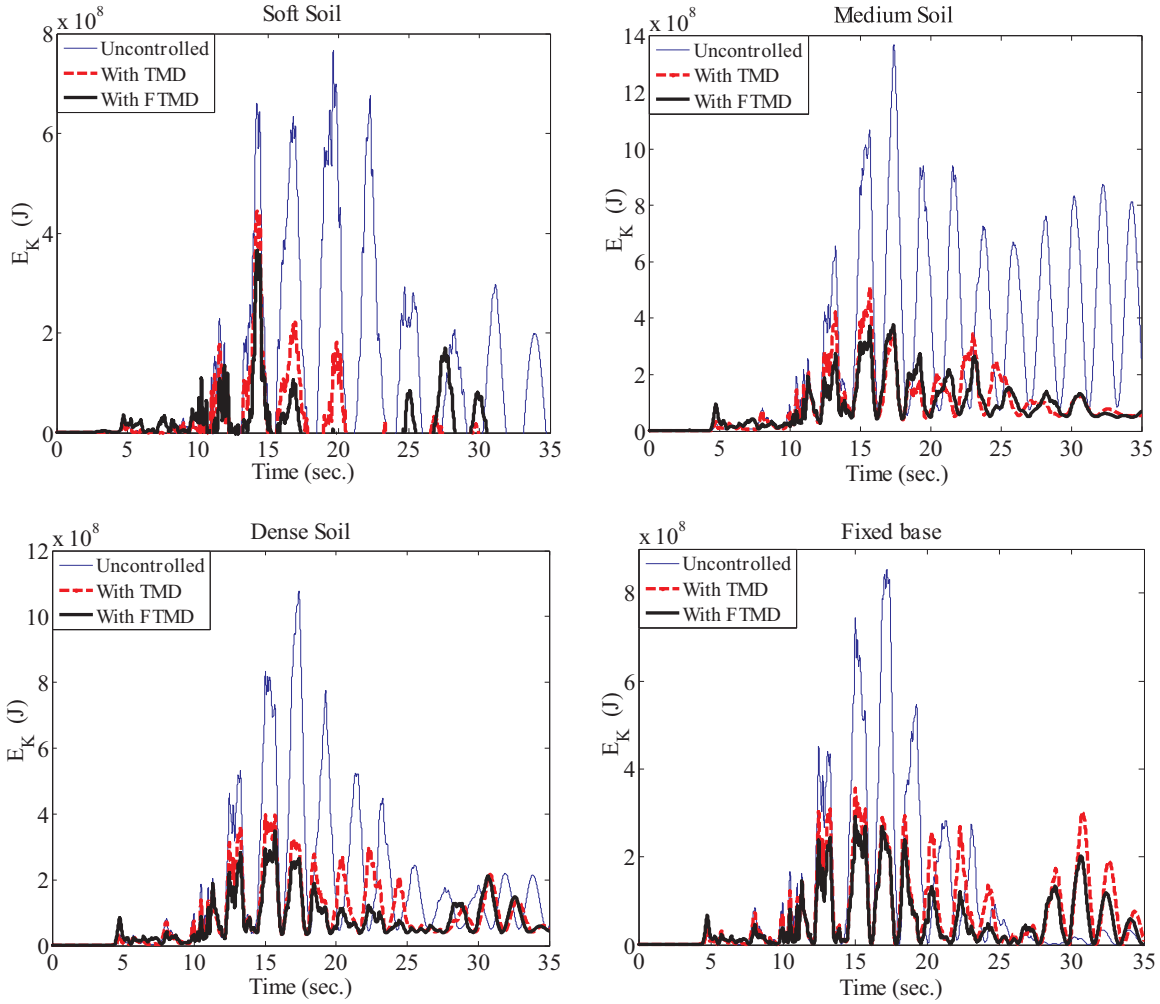

Fig. 7. Time histories of the kinetic energy during Tabas earthquake for different conditions of the ground.

and FTMD, the mass ratio $\gamma = 0.05$ is preselected for both TMD and FTMD.

Similar to other heuristic optimization techniques, it is important to tune the algorithm parameters to achieve sensible results. Selecting a small value of p_a allows a wider range of search space and reduces the risk of being trapped in local optimizations, although it increases computational efforts. On the other hand, the population size n is selected based on the optimization problem. Increasing the population size increases the computational efforts and running time. A value of the population size is capable of giving favorable results and selecting a larger population size while increasing the computational time may produce the same results that are obtained with a fewer population size. Based on the experience of the authors, a different range of the effective parameters of CS, including population size n and the discovery probability p_a, is tested for the tackled problems. The best values of the parameters are found as $n = 25$, $p_a = 0.25$ for optimum tuning of TMD; and $n = 35$, $p_a = 0.25$ for optimum tuning of FTMD.

The simulation and time history analyses of the structure are carried out using MATLAB/Simulink software [53]. Considering four earthquake accelerograms, including Tabas, Bam, Kobe, and Chi-Chi earthquakes, as shown in Fig. 2, the optimal parameters of TMD and FTMD for a preselected mass ratio $\gamma = 0.05$ are tuned using the MOCS for three types of soil (soft, medium, and dense) and the fixed-base case. Considering the building subjected to Tabas earthquake, the Pareto-optimal front diagrams for optimum tuning of the TMD and FTMD parameters are illustrated in Fig. 3. It can be seen the MOCS generates a set of possible solutions for designers, which form the so-called Pareto front. Each member of the Pareto front can be represented by a vector in the design space. The strategy used in this paper for finding the best optimal tuning of TMD and FTMD from the Pareto-optimal front diagram is based on selecting a design vector so that it gives the maximum reduction in the maximum floor displacement without any increase in the maximum floor acceleration of the structure in comparison with the corresponding responses in the uncontrolled structure.

Table 3 shows the values of the optimum parameters of TMD and FTMD obtained from the optimum design process based on MOCS.

5. Results and discussion

Considering the structure on the fixed base and three types of soil, the time history analyses of the structure are carried out during four earthquake excitations and the performances of the FTMD and TMD tuned using the MOCS are discussed for different conditions of the ground. Considering the Tabas earthquake as an example, the time histories of the top floor displacement of the structure equipped with TMD and FTMD are compared with different conditions of the ground in Fig. 4. The time responses corresponding to the uncontrolled structure are also shown in the figure. The maximum drifts of floors during the Tabas earthquake are shown in Fig. 5. It can be seen, the TMD and FTMD are able to reduce the maximum floor displacement of the studied building. During the Tabas earthquake, the maximum top floor displacements of the uncontrolled structure are about 4.23, 2.67, 2.26, and 2.02 m for soft, medium, dense, and the fixed base state, respectively, whereas these responses are about 3.06, 1.50, 1.28, and 1.18 m

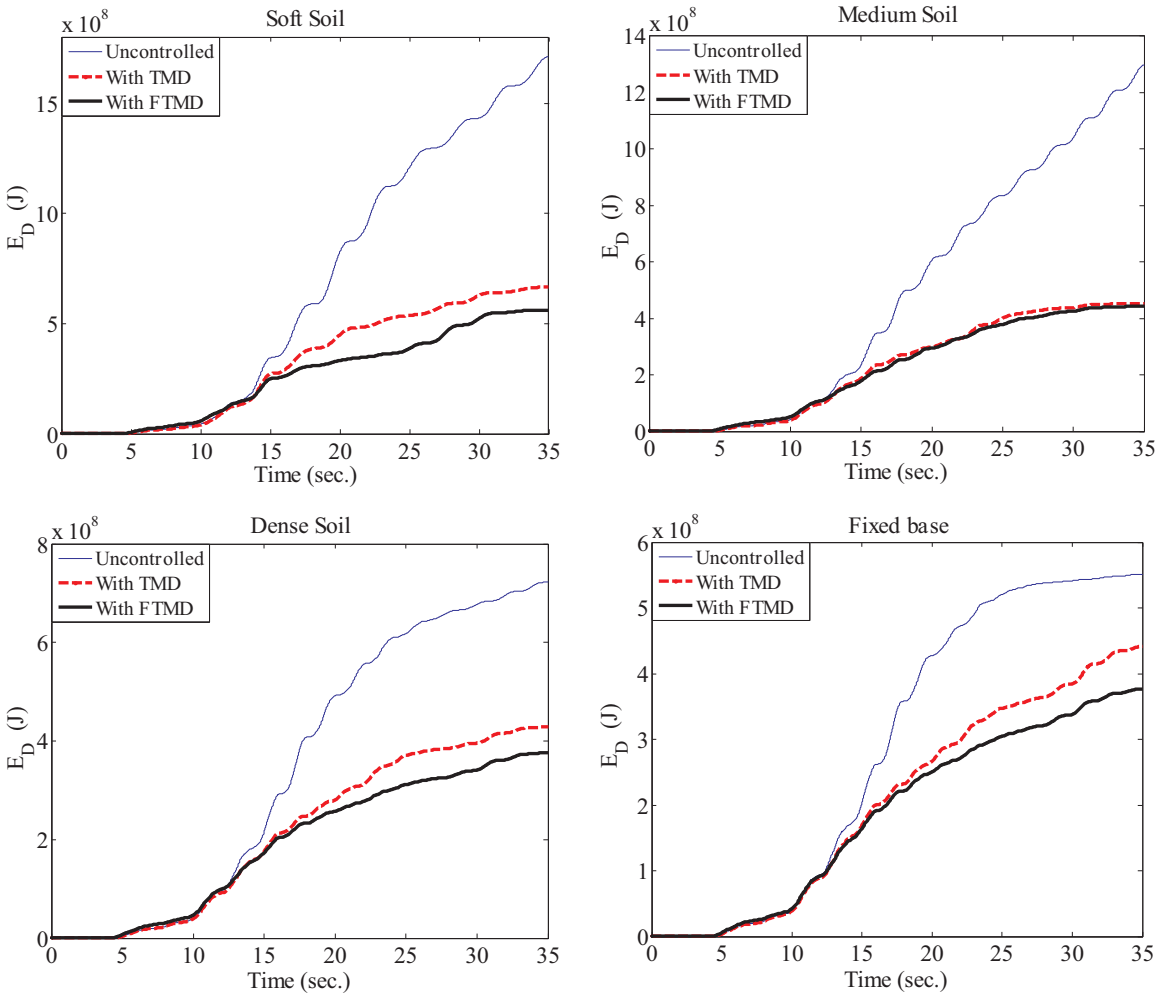

Fig. 8. Time histories of the damping energy during Tabas earthquake for different conditions of the ground.

for the structure equipped with TMD and 2.29, 1.19, 1.03, and 1.01 m for the structure equipped with FTMD, respectively. Hence, the TMD results in a reduction of 28%, 44%, 43%, and 42%, while the FTMD device provides a reduction of 46%, 55%, 54%, and 50% in comparison with the uncontrolled structure, respectively. In addition, it is concluded that the TMD and FTMD are more effective in the structure on hard soils. Fig. 5 indicates that the TMD and FTMD give a proper performance in the reduction of maximum drift of floors. The superiority of the FTMD with respect to the TMD in the reduction of drift of floors is also found.

Table 4 represents the maximum floor displacement, acceleration, and drift of floors of the studied structure subjected to the Tabas, Bam, Kobe, and Chi-Chi earthquakes. The results are given for the fixed-base and three types of soils i.e. soft, medium and dense. The percentages of reductions in comparison with the corresponding uncontrolled cases are also inserted in the table. The results show that the time responses of the structure are significantly affected by the soil type. In other words, ignoring the SSI effects may result in an inappropriate and unrealistic estimation of the seismic responses of high-rise structures. It can be observed that the TMD mitigates the seismic responses in terms of peak floor displacement and drift; however, it may not have a significant effect in some earthquake excitations such as Bam and Chi-Chi earthquakes. In fact, since the parameters of a passive control device, such as TMD devices, are constant values, they are unable to adequately cope with variations in induced loads of earthquake or changes in structural dynamic properties and thus their performance is limited. Alternatively stated, the seismic performance and behavior of the structures equipped with TMD are affected by intensity and frequency content of the excitation [54]. For example, for the Chi-Chi earthquake, the TMD results in 11%, 10%, 10%, and 9% reduction in the peak floor displacement for the cases of soft, medium, and dense soils and the fixed base case, respectively, while the FTMD provides a better performance in reducing the peak top floor displacement in most earthquakes for different conditions of the ground. In the Chi-Chi earthquake, the FTMD gives a reduction of 32%, 22%, 27%, and 49% in the terms of the peak floor displacement, respectively. Similarly, the simulation results indicate that the FTMD performs better than TMD in reduction of maximum drift of floors, so that the TMD reduces the maximum drift of floors during the Chi-Chi earthquake about 9%, 9%, 8%, and 7% in comparison with the uncontrolled cases, while these reductions are obtained about 28%, 19%, 30% and 42% for the FTMD in different conditions of the ground. Therefore, it is concluded that the FTMDs are more advantageous devices than that the TMD for vibration mitigation of the seismic-excited high–rise buildings. The results also show that the FTMD has a better performance in reducing the maximum floor acceleration of the structure. The results reveal the importance of considering SSI effects in the design process of the TMD and FTMD parameters. It is found that the efficiency of the TMD and FTMD is often decreased in soft soils. In other words, their performances are usually impaired by increasing the soil softness. So, ignoring the SSI effects in the modeling of the structure may result in incorrect and unrealistic time responses and performances of TMD and FTMD in tall structures.

In order to achieve an overall conclusion, the average reduction values of the maximum structural responses for all studied earthquakes

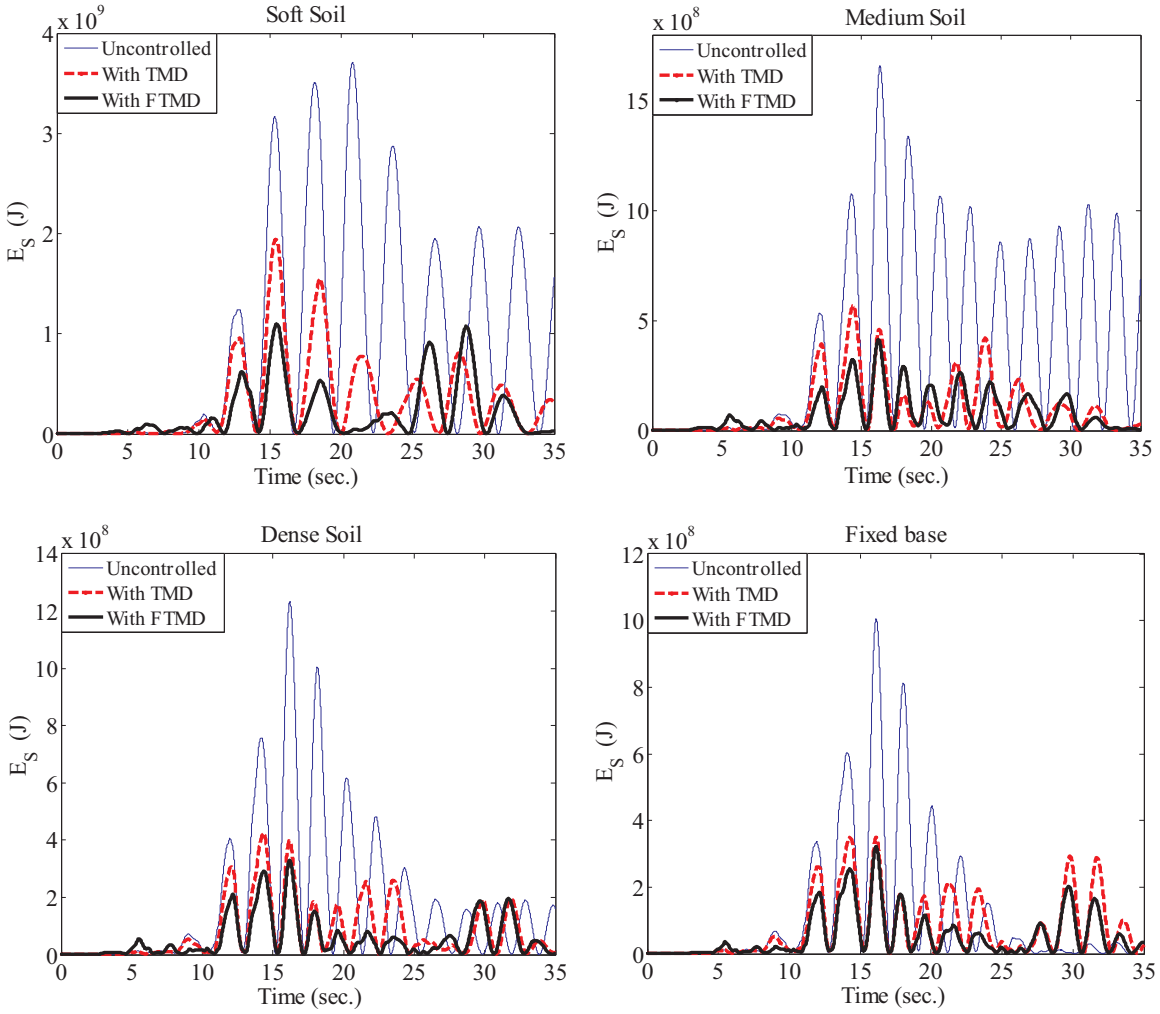

Fig. 9. Time histories of the strain energy during Tabas earthquake for different conditions of the ground.

with respect to the corresponding uncontrolled cases are indicated in Table 5. The results are represented in the cases of three types of soils and fixed-base. It can be seen, FTMD significantly provides a better performance in reducing the maximum floor displacement and drift of the building in all condition of the ground. According to the overall results, TMDs and FTMDs are more effective for the structures on hard soils and their efficiency is degraded in soft soils.

It is interesting to evaluate the efficiency of TMD and FTMD systems for vibration control of the tall buildings from the energy point of view. Seismic control of a structure can be described as an energy transfer process. Seismic input energy (E_I) entering the main structure is converted to both recoverable strain (E_S) and relative kinetic (E_K) energies. Also, some amount of the input energy is dissipated by the damping energy (E_D). The sum of the relative kinetic and recoverable strain energies is known as the total energy of the system or the damage energy. The time histories of the seismic input energy of the main structure during the Tabas earthquake for the cases of uncontrolled, equipped with TMD, and equipped with FTMD are illustrated in Fig. 6. Similarly, Figs. 7–9 depict the time histories of the relative kinetic, damping and recoverable strain energies of the main structure for different conditions of the ground. Table 6 also summarizes the maximum values of the various energy forms for different earthquake excitations and soil types. Fig. 6 indicates that the maximum values of the seismic input energy of the main structure equipped with the TMD and FTMD are smaller than those given for the uncontrolled structure. This result arises from the fact that a significant amount of the seismic input energy is dissipated by the TMD and FTMD and a small portion of the input energy is transferred to the main structure. As it can be seen from Table 6, the TMD results in reduction of 29%, 24%, 20%, and 17% in soft, medium, and dense soil and fixed-base cases, respectively. Similarly, the FTMD provides a better performance than the TMD and leads to reduction of 49%, 37%, 25%, and 24%, respectively. Figs. 7–9 also show that the damping energies of the structures equipped with TMD and FTMD are reduced, whereas the kinetic and strain energies of the structures are effectively reduced in comparison with the uncontrolled structure. This means that the seismic damage energy of the building using TMD and FTMD is reduced in comparison with the uncontrolled building.

The averages of reductions of the maximum values of the various energy forms for all studied earthquakes for different soil types are summarized in Table 7. The TMD results in reduction of 9%, 11%, 10%, and 30% in comparison with the uncontrolled structure in term of the maximum seismic input energy for soft, medium, and dense soil and fixed-base conditions, while these reductions are respectively given about 26%, 26%, 31%, and 53% for the FTMD. The damping energy is increased slightly when the TMD or FTMD is used. However, the reduction of the kinetic and strain energies confirms that TMDs and FTMDs are capable of mitigating the seismic damage in tall structures. It can be seen that the reductions of kinetic energy are about 14%, 27%, 27% and 27% for soft, medium, and dense soil and the fixed-base conditions when TMD is employed, while the FTMD performs better than TMD in reducing the corresponding energies, and it provides a reduction of 30%, 40%, 43%, and 65%. Considering the strain energies, the reductions are given as much as 22%, 31%, 29%, and 28% for the

Table 6
Maximum values of the various energy forms for different soils.

			Maximum Energy (J)			Reduction (%)	
Earthq.	**Soil type**	**Energy**	**Unctrl.**	**TMD**	**FTMD**	**TMD**	**FTMD**
Tabas	Soft	E_K	7.66 e8	4.44 e8	3.66 e8	42.04	52.22
		E_D	1.58 e9	6.51 e8	5.56 e8	58.70	64.81
		E_S	3.71 e9	1.94 e9	1.10 e9	47.71	70.35
		E_I	2.43 e9	1.73 e9	1.24 e9	28.81	48.97
	Medium	E_K	1.37 e9	5.10 e8	3.78 e8	62.77	71.75
		E_D	1.20 e9	4.51 e8	4.40 e8	62.42	63.33
		E_S	1.66 e9	5.70 e8	4.15 e8	65.66	75.00
		E_I	1.90 e9	1.44 e9	1.19 e9	24.21	37.37
	Dense	E_K	1.08 e9	3.98 e8	3.50 e8	63.15	67.59
		E_D	7.04 e8	4.22 e8	3.70 e8	40.06	47.44
		E_S	1.23 e9	4.22 e8	3.30 e8	65.69	73.17
		E_I	1.53 e9	1.23 e9	1.14 e9	19.61	25.49
	Fixed base	E_K	8.53 e8	3.57 e8	2.91 e8	58.15	65.89
		E_D	5.48 e8	4.29 e8	3.69 e8	21.72	32.66
		E_S	1.01 e9	3.50 e8	3.22 e8	65.35	68.12
		E_I	1.33 e9	1.11 e9	1.01 e9	16.54	24.06
Bam	Soft	E_K	4.44 e7	4.44 e7	3.35 e7	0.00	24.55
		E_D	9.17 e7	7.18 e7	9.40 e7	21.70	-2.51
		E_S	5.43 e7	4.89 e7	4.04 e7	9.94	25.60
		E_I	1.02 e9	1.01 e9	7.83 e8	0.98	23.24
	Medium	E_K	8.79 e7	8.62 e7	7.70 e7	1.93	12.40
		E_D	1.08 e8	6.39 e7	1.08 e8	40.83	0.00
		E_S	4.97 e7	4.39 e7	3.45 e7	11.67	30.58
		E_I	1.17 e9	1.16 e9	1.03 e9	0.85	11.97
	Dense	E_K	9.59 e7	9.51 e7	8.25 e7	0.83	13.97
		E_D	1.03 e8	8.34 e7	8.11 e7	19.03	21.26
		E_S	4.82 e7	4.43 e7	3.78 e7	8.09	21.57
		E_I	1.19 e9	1.18 e9	1.04 e9	0.84	12.61
	Fixed base	E_K	1.00 e8	9.90 e7	7.34 e7	1.00	26.6
		E_D	9.94 e7	7.66 e7	1.10 e8	22.94	-10.66
		E_S	4.71 e7	4.27 e7	3.43 e7	9.34	27.18
		E_I	1.20 e9	1.22 e8	8.14 e8	89.83	32.16
Kobe	Soft	E_K	1.58 e8	1.57 e8	1.56 e8	0.63	1.27
		E_D	1.52 e8	1.41 e8	1.36 e8	7.23	10.53
		E_S	8.04 e7	7.27 e7	5.93 e7	9.58	26.24
		E_I	1.97 e8	1.93 e8	1.90 e8	2.03	3.55
	Medium	E_K	1.36 e8	1.21 e8	9.58 e7	11.03	29.56
		E_D	1.86 e8	1.70 e8	1.59 e8	8.60	14.52
		E_S	1.22 e8	8.88 e7	5.53 e7	27.21	54.67
		E_I	2.45 e8	2.25 e8	1.70 e8	8.16	30.16
	Dense	E_K	1.43 e8	1.21 e8	1.05 e8	15.38	26.57
		E_D	1.98 e8	1.71 e8	1.60 e8	13.63	19.19
		E_S	1.19 e8	8.94 e7	4.82 e7	24.87	59.50
		E_I	2.54 e8	2.30 e8	1.53 e8	9.45	39.76
	Fixed base	E_K	1.38 e8	1.12 e8	8.56 e6	18.84	93.80
		E_D	2.02 e8	1.75 e8	1.50 e7	13.37	92.57
		E_S	1.15 e8	8.85 e7	5.48 e6	23.04	95.23
		E_I	2.58 e8	2.42 e8	1.83 e7	6.20	92.91
Chi -Chi	Soft	E_K	5.42 e8	4.71 e8	3.15 e8	13.10	41.88
		E_D	7.55 e8	1.40 e9	6.70 e8	85.43-	11.26
		E_S	3.04 e9	2.44 e9	1.47 e9	19.74	51.64
		E_I	1.58 e10	1.53 e10	1.11 e10	3.16	29.75
	Medium	E_K	1.42 e9	9.63 e8	7.45 e8	32.18	47.54
		E_D	1.57 e9	7.87 e8	3.90 e8	49.87	75.16
		E_S	1.61 e9	1.31 e9	1.00 e9	18.63	37.89
		E_I	1.83 e10	1.66 e10	1.38 e10	9.29	24.59
	Dense	E_K	1.53 e9	1.07 e9	5.23 e8	30.07	65.82
		E_D	1.30 e9	7.61 e8	7.38 e8	41.46	43.23
		E_S	1.39 e9	1.15 e9	6.90 e8	17.27	50.36
		E_I	1.79 e10	1.62 e10	9.64 e9	9.50	46.15
	Fixed base	E_K	1.56 e9	1.12 e9	4.06 e8	28.21	73.97
		E_D	1.20 e9	7.12 e8	7.77 e8	40.67	35.25
		E_S	1.25 e9	1.05 e9	3.22 e8	16.00	74.24
		E_I	1.73 e10	1.58 e10	6.73 e9	8.68	61.10

main structures equipped with TMD and 43%, 50%, 51%, and 66% for the main structures equipped with FTMD. Furthermore, the overall results show an increased trend in the amount of seismic input and damage energies by increasing the soil softness. So, ignoring the SSI effects may result in an incorrect and unrealistic estimation of the performance of TMD and FTMD from the energy point of view.

6. Conclusions

The effectiveness of TMD and FTMD for seismic control of a 40-story building with a height-to-width ratio of 4, including SSI effects, was investigated in the present study. Different conditions of the ground including soft, medium, and dense soils and the fixed-base case were

Table 7
The averages of reductions of the maximum energies for all studied earthquakes.

Soil type	Energy	Reduction of maximum energy (%)	
		TMD	FTMD
Soft	E_K	13.94	29.98
	E_D	0.55	21.22
	E_S	21.74	43.46
	E_I	8.75	26.38
Medium	E_K	26.98	40.31
	E_D	40.43	38.25
	E_S	30.79	49.54
	E_I	10.63	26.02
Dense	E_K	27.36	43.49
	E_D	28.55	32.78
	E_S	28.98	51.15
	E_I	9.85	31.00
Fixed base	E_K	26.55	65.07
	E_D	24.68	37.46
	E_S	28.43	66.19
	E_I	30.31	52.56

considered for numerical studies. A MOCS algorithm was applied to tune the optimum parameters of the TMD and FTMD. Results showed that ignoring the SSI effects might result in an unrealistic estimation of seismic responses and performance of the TMD and FTMD in the high-rise structure subjected to near-field earthquakes. Moreover, it was found that the FTMD gave a better performance in reducing the seismic responses in terms of the maximum displacement, acceleration, and drift. In addition, the performance of FTMD in comparison with TMD during f earthquakes was investigated from the energy point of view. The simulation results indicated that the FTMD performed better than the TMD for mitigation of seismic input energy to the main structure. Furthermore, the results demonstrated that the damping energy of the main structure was reduced by employing the TMD or FTMD. Nevertheless, a significant reduction resulted in the amounts of the kinetic and strain energies of the main structure in comparison with those given for the uncontrolled structure. The results showed the superiority of the FTMD in reducing the maximum kinetic and strain energies of the main structure, which confirmed that the FTMD can reduce the seismic damage energy entering to the tall buildings better than the TMD during near-field earthquakes. The maximum seismic input and damage energies of the main structures were often increased by increasing the softness of the soil. Hence, ignoring the SSI effects might give unrealistic results about the performances of TMD and FTMD in mitigation of seismic damages during near-field earthquakes.

In the present study, four earthquake excitations were selected for numerical studies. Although the optimum design of a TMD for seismic-excited structures has received much attention from researchers, finding the reliable and robust design strategies of TMD/FTMD subjected to different earthquake excitations is an open problem. Meanwhile, some studies have been addressed this challenging task to TMDs which may be suitable strategies for the design of FTMD. Considering the possible uncertainty in the earthquake load, a reliability-based design optimization (RBDO) scheme is able to give a reliable and robust design of TMD parameters [55,56]. Additionally, a random-based acceleration, modeled by a stationary filtered white noise process, can be considered instead of different earthquake excitations in the optimum design process of TMD parameters [28,29,36]. Recently, a continuous stationary critical excitation as the most severe earthquake has been taken into account for the optimal design of TMD [57]. Access to reliable and robust design strategies of FTMD for different seismic excitations is an important topic that still inspires the efforts of researchers for further studies.

References

[1] Bekdaş G, Nigdeli SM. Estimating optimum parameters of tuned mass dampers using harmony search. Eng Struct 2011;33:2716–23.
[2] Bakre S, Jangid R. Optimum parameters of tuned mass damper for damped main system. Struct Control Health Monit 2007;14:448–70.
[3] Ghosh A, Basu B. A closed-form optimal tuning criterion for TMD in damped structures. Struct Control Health Monit 2007;14:681–92.
[4] Leung A, Zhang H. Particle swarm optimization of tuned mass dampers. Eng Struct 2009;31:715–28.
[5] Salvi J, Rizzi E, Moens D, Jonckheere S. A numerical approach towards best tuning of tuned mass dampers. In Proceedings of the 25th international conference on noise and vibration engineering (ISMA 2012), Leuven, Belgium; 2012, pp. 19.
[6] Greco R, Marano GC. Optimum design of tuned mass dampers by displacement and energy perspectives. Soil Dyn Earthq Eng 2013;49:243–53.
[7] Etedali S, Mollayi N. Cuckoo search-based least squares support vector machine models for optimum tuning of tuned mass dampers. Int J Struct Stab Dyn 2018;18:1850028.
[8] Hadi MN, Arfiadi Y. Optimum design of absorber for MDOF structures. J Struct Eng 1998;124:1272–80.
[9] Sadek F, Mohraz B, Taylor AW, Chung RM. A method of estimating the parameters of tuned mass dampers for seismic applications. Earthq Eng Struct Dyn 1997;26:617–36.
[10] Kaveh A, Mohammadi S, Hosseini OK, Keyhani A, Kalatjari V. Optimum parameters of tuned mass dampers for seismic applications using charged system search, Iranian Journal of Science and Technology. Trans Civil Eng 2015;39:21–40.
[11] Salvi J, Rizzi E. Optimum tuning of tuned mass dampers for frame structures under earthquake excitation. Struct Control Health Monit 2015;22:707–25.
[12] Giuliano F. Note on the paper “Optimum parameters of tuned liquid column–gas damper for mitigation of seismic-induced vibrations of offshore jacket platforms” by Seyed Amin Mousavi, Khosrow Bargi, and Seyed Mehdi Zahrai. Struct Control Health Monit 2013;20:852.
[13] Farshidianfar A, Soheili S. Ant colony optimization of tuned mass dampers for earthquake oscillations of high-rise structures including soil-structure interaction. Soil Dyn Earthq Eng 2013;51:14–22.
[14] Khatibinia M, Gholami H, Labbafi S. Multi-objective optimization of tuned mass dampers considering soil-structure interaction. Int J Optim Civil Eng 2016;6:595–610.
[15] Shourestani S, Soltani F, Ghasemi M, Etedali S. SSI effects on seismic behavior of smart base-isolated structures. Geomech Eng 2018;14:161–74.
[16] Jabary R, Madabhushi S. Structure-soil-structure interaction effects on structures retrofitted with tuned mass dampers. Soil Dyn Earthq Eng 2017;100:301–15.
[17] Rahai AR, Saberi H, Saberi H. A Discussion of the paper: “ant colony optimization of tuned mass dampers for earthquake oscillations of high-rise structures including soil-structure interaction” [Soil Dyn. Earthq. Eng. 51 (2013) 14–22]. Soil Dyn Earthq Eng 2017:263–5.
[18] Jabary R, Madabhushi S. Tuned mass damper effects on the response of multi-storied structures observed in geotechnical centrifuge tests. Soil Dyn Earthq Eng 2015;77:373–80.
[19] Bekdaş G, Nigdeli SM. Metaheuristic based optimization of tuned mass dampers under earthquake excitation by considering soil-structure interaction. Soil Dyn Earthq Eng 2017;92:443–61.
[20] Chen G, Wu J. Optimal placement of multiple tune mass dampers for seismic structures. J Struct Eng 2001;127:1054–62.
[21] Lukkunaprasit P, Wanitkorkul A. Inelastic buildings with tuned mass dampers under moderate ground motions from distant earthquakes. Earthq Eng Struct Dyn 2001;30:537–51.
[22] Pinkaew T, Lukkunaprasit P, Chatupote P. Seismic effectiveness of tuned mass dampers for damage reduction of structures. Eng Struct 2003;25:39–46.
[23] Matta E. Effectiveness of tuned mass dampers against ground motion pulses. J Struct Eng 2012;139:188–98.
[24] Bray JD, Rodriguez-Marek A. Characterization of forward-directivity ground motions in the near-fault region. Soil Dyn Earthq Eng 2004;24:815–28.
[25] Matta E. Performance of tuned mass dampers against near-field earthquakes. Struct Eng Mech 2011;39:621–42.
[26] Samali B, Al-Dawod M. Performance of a five-storey benchmark model using an active tuned mass damper and a fuzzy controller. Eng Struct 2003;25:1597–610.
[27] Pourzeynali S, Lavasani H, Modarayi A. Active control of high rise building structures using fuzzy logic and genetic algorithms. Eng Struct 2007;29:346–57.
[28] Heidari AH, Etedali S, Javaheri-Tafti MR. A hybrid LQR-PID control design for seismic control of buildings equipped with ATMD. Front Struct Civil Eng 2017:1–14.
[29] Etedali S, Tavakoli S. PD/PID controller design for seismic control of high-rise buildings using multi-objective optimization: a comparative study with LQR controller. J Earthq Tsunami 2017;11:1750009.
[30] Nazarimofrad E, Zahrai SM. Fuzzy control of asymmetric plan buildings with active tuned mass damper considering soil-structure interactionFuzzy control of asymmetric plan buildings with active tuned mass damper considering soil-structure interaction. Soil Dyn Earthq Eng 2018;115:838–52.
[31] Etedali S, Zamani AA, Tavakoli S, GBMO-based A. PI $^{\lambda}D^{\mu}$ controller for vibration mitigation of seismic-excited structures. Autom Constr 2018;87:1–12.
[32] Sun C, Nagarajaiah S. Study on semi-active tuned mass damper with variable damping and stiffness under seismic excitations. Struct Control Health Monit 2014;21:890–906.
[33] Kim HS, Chang C, Kang JW. Control performance evaluation of semi-active TMD

subjected to various types of loads. Int J Steel Struct 2015;15:581–94.
[34] Gewei Z, Basu B. A study on friction-tuned mass damper: harmonic solution and statistical linearization. J Vib Control 2011;17:721–31.
[35] Pisal AY, Jangid R. Seismic response of multi-story structure with multiple tuned mass friction dampers. Int J Adv Struct Eng 2014;6:1–13.
[36] Shahi M, Sohrabi MR, Etedali S. Seismic control of high-rise buildings equipped with ATMD including soil-structure interaction effects. J Earthq Tsunami 2018;12:1850010.
[37] Bhaskararao A, Jangid R. Seismic analysis of structures connected with friction dampers. Eng Struct 2006;28:690–703.
[38] Yang XS, Deb S. Cuckoo search via Lévy flights, in: Nature & Biologically Inspired Computing, 2009. NaBIC 2009. World Congress on, IEEE; 2009, p. 210–214.
[39] Rajabioun R. Cuckoo optimization algorithm. Appl Soft Comput 2011;11:5508–18.
[40] Yang XS, Deb S. Cuckoo search: recent advances and applications. Neural Comput Appl 2014;24:169–74.
[41] Yang XS, Deb S. Multiobjective cuckoo search for design optimization, computers and operations research. 2013;40:1616–24.
[42] Civicioglu P, Besdok E. A conceptual comparison of the Cuckoo-search, particle swarm optimization, differential evolution and artificial bee colony algorithms. Artif Intell Rev 2013:315–46.
[43] Gandomi AH, Talatahari S, Yang XS, Deb S. Design optimization of truss structures using cuckoo search algorithm. Struct Des Tall Spec Build 2013;22:1330–49.
[44] Samani MZ, Amini F. A cuckoo search controller for seismic control of a benchmark tall building. J Vibroeng 2015;17. [1601].
[45] Etedali S, Tavakoli S, Sohrabi MR. Design of a decoupled PID controller via MOCS for seismic control of smart structures. Earthq Struct 2016;10:1067–87.
[46] Zamani AA, Tavakoli S, Etedali S, Sadeghi J. Adaptive fractional order fuzzy proportional–integral–derivative control of smart base-isolated structures equipped with magnetorheological dampers. J Intell Mater Syst Struct 2018;29(5):830–44.
[47] Zamani AA, Tavakoli S, Etedali S. Control of piezoelectric friction dampers in smart base-isolated structures using self-tuning and adaptive fuzzy proportional–derivative controllers. J Intell Mater Syst Struct 2017;28:1287–302.
[48] Zamani AA, Tavakoli S, Etedali S. Fractional order PID control design for semi-active control of smart base-isolated structures: a multi-objective cuckoo search approach. ISA Trans 2017;67:222–32.
[49] Keshtegar B, Etedali S. Novel mathematical models based on regression analysis scheme for optimum tuning of TMD parameters. J Solid Fluid Mech 2017;6:59–75.
[50] Etedali S. A new modified independent modal space control approach toward control of seismic-excited structures. Bull Earthq Eng 2017;15:4215–43.
[51] Zamani AA, Tavakoli S, Etedali S, Sadeghi J. Online tuning of fractional order fuzzy PID controller in smart seismic isolated structures. Bull Earthq Eng 2018;16:3153–70.
[52] Liu MY, Chiang WL, Hwang JH, Chu CR. Wind-induced vibration of high-rise building with tuned mass damper including soil–structure interaction. J Wind Eng Ind Aerodyn 2008;96:1092–102.
[53] MATLAB. The Math Works, Inc., Natick, MA; 2000.
[54] De Silva CW. Vibration damping, control, and design. CRC Press; 2007.
[55] Gholizad A, Mohammadi SD Ojaghzadeh. Reliability-based design of tuned mass damper using Monte Carlo simulation under artificial earthquake records. Int J Struct Stab Dyn 2017;17:1750121.
[56] Rathi AK, Chakraborty A. Reliability-based performance optimization of TMD for vibration control of structures with uncertainty in parameters and excitation. Struct Control Health Monit 2017;24:e1857.
[57] Kamgar R, Samea P, Khatibinia M. Optimizing parameters of tuned mass damper subjected to critical earthquake. Struct Des Tall Spec Build 2018;27:e1460.